Chemical-Looping Combustion in Packed-Fluidized Bed Reactor – Fundamental Modeling and Batch Experiments with Random Metal

energy&fuels

pubs.acs.org/EF

Article

Chemical Looping Combustion in a Packed Fluidized Bed Reactor—Fundamental Modeling and Batch Experiments with Random Metal Packings

Nasrin Nemati,* Yukari Tsuji, Tobias Mattisson, and Magnus Rydén

Cite This: https://doi.org/10.1021/acs.energyfuels.2c00527

Read Online

ACCESS | Metrics & More | Article Recommendations | Supporting Information

ABSTRACT: The conversion of gaseous fuels during chemical looping combustion (CLC) was investigated in a packed fluidized reactor. The experimental setup consisted of a cylindrical laboratory-scale bubbling fluidized bed reactor with an inner diameter of 78 mm and a height of 1.27 m. Two types of fuel, syngas (50:50% H_2/CO) and carbon monoxide (100% CO), were used. Two different types of packings were assessed and compared to the reference case, which was a bubbling bed with no packings. The investigated packings were 25 mm stainless-steel thread saddle rings (RMSR) with a bulk density of 195 kg/m^3 and 25 mm stainless-steel pall rings (Hiflow) with a bulk density of 271 kg/m^3. The height of the packed reactor section was kept constant at 1 m. Ilmenite concentrate particles in the size range of 90−212 μm was used as an oxygen carrier. The unfluidized bed height was varied between 10 and 60 cm. The results show that the fuel conversion increases as the bed height increases and that the use of packings have a positive effect on fuel conversion. For RMSR packings, the syngas conversion at 840 °C improves from 0.84 (for 10 cm bed height) to 1.00 (for 60 cm bed height). This should be compared to the bed with no packings, for which the corresponding improvement was from 0.69 to 0.98. The general pattern is consistent for all fuels, packings, and bed heights. The results are interpreted as an improvement in gas−solid mass transfer when packings are used, mainly as a result of the reduced bubble size. A fundamental analysis of the variance in the pressure drop over the bed to estimate the bubble diameter supports this interpretation. It is also shown that the mass-based first-order effective reaction contact factor k_f improves up to 109% in the bed with RMSR packings compared to the bed without packings.

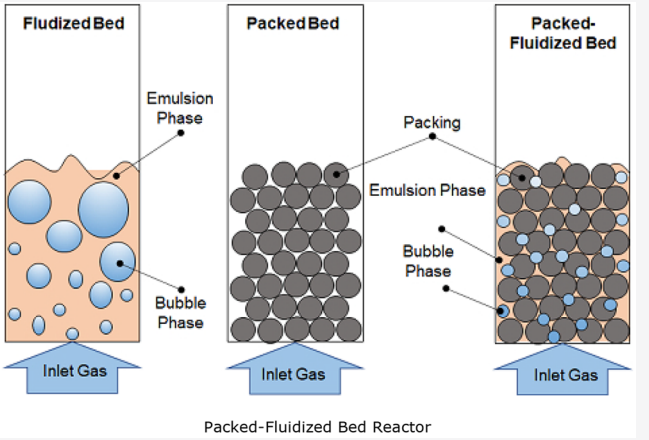

Packed-Fluidized Bed Reactor

1. INTRODUCTION

Reducing CO_2 emissions is an urgent matter to mitigate the environmental effects expected from global warming. One of the methods available to decrease CO_2 emissions is carbon capture and storage (CCS).[1] According to some climate models, generation of so-called negative emissions is currently the only way to achieve the global goal of limiting global warming to below 2 °C.[2] Negative emissions could be realized, e.g., by applying CO_2 capture during biomass conversion processes.[3−5] This is because the biomass has absorbed CO_2 from the atmosphere during its growth. Thus, capturing CO_2 from biomass utilization and preventing it from reaching the atmosphere results in net-negative emissions. The viability of different CO_2 separation concepts has been recognized, and many CCS projects have been launched all over the world in the past decades.[6]

There are several gas separation technologies available for CO_2 capture, such as, for example, amine scrubbing and oxy-fuel combustion. Each technology has strengths and weaknesses in terms of cost, efficiency, and applicability.[7] Chemical looping combustion (CLC) is one technology that could potentially reduce costs significantly, because no gas separation step is needed to obtain pure CO_2 in the flue gases.[8−12] Most often, CLC uses interconnected fluidized bed reactors. When this reactor setup is used, it is important to achieve high and uniform gas−solid mass transfer. This is because transport of fuel gases to the surface of the bed material is a necessary step to allow for fuel conversion in CLC. This paper explores a novel and straightforward method to improve the performance of bubbling fluidized bed (BFB) reactors in CLC. It involves

Special Issue: 2022 Pioneers in Energy Research: Anders Lyngfelt

Received: February 23, 2022
Revised: May 5, 2022

the utilization of random metal packings to improve the gas−solid mass transfer by reducing the bubble size and growth.

2. BACKGROUND

2.1. CLC. The fundamental principle of CLC is the utilization of two separate but interconnected reactors, usually referred to as the air reactor (AR) and the fuel reactor (FR). A simplified schematic description of CLC is shown in Figure 1.

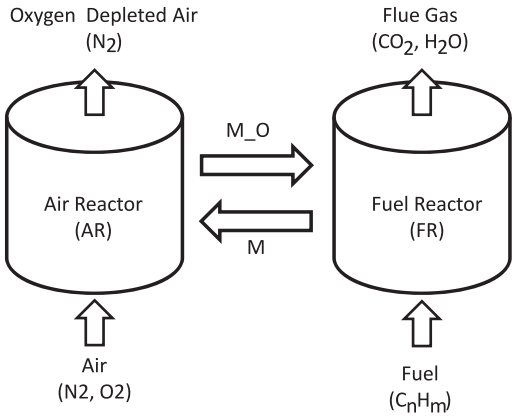

Figure 1. Schematic description of CLC.

As depicted in Figure 1, a solid metal oxide commonly referred to as the oxygen carrier (M_O) transports oxygen between the two reactors. The oxygen carrier will react with and oxidize the fuel (C_nH_m) in the FR. The products are a reduced oxygen carrier (M) and CO_2 and H_2O as flue gas. CO_2 capture in this system would be more easily accomplished in comparison to conventional combustors, because the flue gas is not diluted with air. Thus, H_2O can be separated from CO_2 by condensation, and there is no need for complex gas separation systems.[13] In the subsequent step, the reduced oxygen carrier is transported to the AR, where it is reoxidized to M_O. The general reduction−oxidation reactions in the FR and AR are described in reactions 1 and 2.

$$C_nH_m + (2n + 0.5m)M\_O \rightarrow nCO_2 + 0.5mH_2O + (2n + 0.5m)M \quad (1)$$

$$M + 0.5O_2 \rightarrow M\_O \quad (2)$$

The CLC process allows for two separate outlet gas flows: one of oxygen depleted air from the AR and one of CO_2 and H_2O from the FR. Pure CO_2 can be obtained simply by cooling the outlet flow from the FR and condensing steam to liquid water. CO_2 capture by conventional gas separation methods results in significant costs and high energy penalty. In contrast, studies have shown that the total cost for CCS with solid fuel by CLC could be as low as 20 € per ton of CO_2.[14]

Reaction 1 describes direct oxidation of a gaseous fuel. When it comes to solid fuel, such as coal or biomass, the reaction pathway becomes more complicated. This is because direct solid−solid reactions are unlikely to occur. One solution to this problem would be to add fuel gasification as a pre-step to the CLC unit.[9] Other possibilities are to apply *in situ* gasification chemical looping combustion (iG-CLC) or chemical looping with oxygen uncoupling (CLOU).[15] In iG-CLC, solid fuel is fed directly to the FR and gasification occurs *in situ* with recirculated exhaust gas (H_2O and CO_2) as fluidizing gas and gasification agent. In CLOU, special type of oxygen carriers are applied, which are capable of releasing gaseous oxygen at the conditions used. Among the latter two options, CLOU has the advantage of reacting much more effortlessly with char and volatiles. Thus, CLOU can avoid char escaping to AR. The drawback with CLOU is the need for more advanced oxygen carriers, e.g., based on CuO.

The general reduction−oxidation reactions for CLOU are described in eqs 3 and 4.[16,17]

$$2M\_O \xrightarrow{\text{uncoupling}} 2M + O_2 \quad (3)$$

$$[\text{char}, C_nH_m, H_2, CO] + O_2 \xrightarrow{\text{combustion}} CO_2 + H_2O \quad (4)$$

Among all of the different designs suggested and studied to realize CLC, the use of fluidized bed (FB) reactors is the design that has gained the most traction. This is due to efficient solid−gas mass transfer, good mixing of particles, and rapid heat transfer, resulting in a relatively homogeneous temperature distribution.[18,19] Many CLC units in the size range from 0.3 kW to 1 MW have been constructed and operated for in total more than 11 000 h, using various types of fuels and oxygen carriers.[9] Thanks to these activities, several challenges that must be faced when upscaling the technology have been identified. These include selection of suitable oxygen carrier materials, improvement of the gas conversion rate in FR, and downstream treatment of flue gas.[8] Other challenges include bubble growth, slugging, and reduced gas−solid mass transfer, and it is these challenges that are addressed in this paper.[20,21]

2.2. Packed Fluidized Beds. Previous studies showed that, in a BFB, the mass transfer rate of gas between the bubble and emulsion phase decreases with an increase in the bubble size.[19−22] While small bubbles are desirable for effective mass transfer, large bubbles can have the opposite effect by causing gas bypass and slugging.[23] One effective method to eliminate bubble growth in BFBs is applying the concept of packed fluidized beds.[22,24,25] In this method, inert stagnant packings of a much larger size than the fluidized particles are applied to inhibit bubble growth and breakdown larger bubbles into smaller bubbles, as illustrated in Figure 2.

Some studies about the use of packed fluidized beds for various applications have been presented in the literature, for example, for examining heat transfer,[26−29] axial dispersion,[30] bed expansion,[31,32] and hydrodynamic behavior of gas−solid beds.[33,34] Through these investigations, it is clear that substantial advantages can be realized by use of a packed fluidized bed.

In CLC, it is critical to achieve a high mass transfer rate between gas and the oxygen carrier throughout the whole bed. In contrast to normal fluidized bed combustion, it cannot be expected that residual combustible components can be converted in the freeboard. Aronsson et al. investigated the effect of using spherical aluminum silicate balls (ASBs) and expanded clay aggregate (ECA) as packings during CLC batch experiments.[22] They observed that these packings can improve fuel conversion. However, they could also result in higher pressure drops inside the bed and particle segregation phenomena.[22,25] Recently, Nemati et al.[20] compared the effect of evolved RMSR packings, simple spherical ASB packings, and a bubbling bed with no packings. It was reported that RMSR can successfully increase the fuel conversion rate compared to ASB and beds with no packings while having limited effect on particle inventory, pressure drop, and solid flux. However,

https://doi.org/10.1021/acs.energyfuels.2c00527
Energy Fuels XXXX, XXX, XXX−XXX

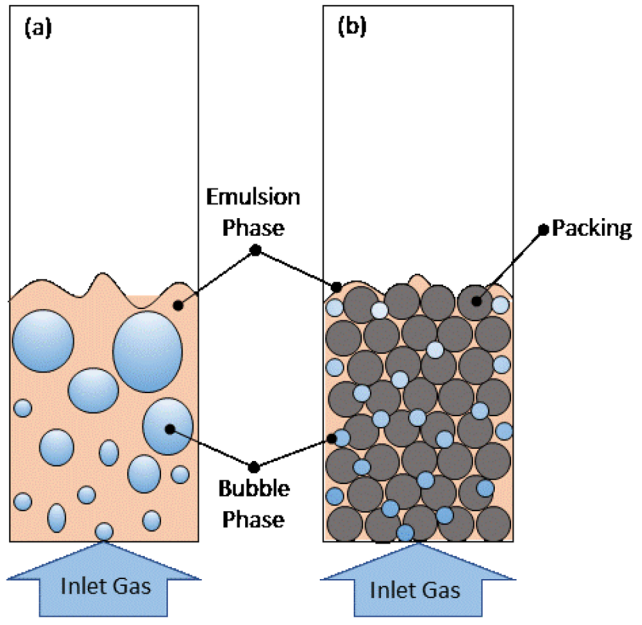

Figure 2. Illustration of (a) conventional BFB and (b) packed fluidized bed.

there is still a lack of investigations for other types of relevant packings, like pall rings (Hiflow), and the theory behind the enhanced fuel conversion.

2.3. Aim of This Study. The aim of the current work is to investigate the impact on the fuel conversion rate and pressure drop of applying two different types of packings, namely, Hiflow and RMSR, to a BFB CLC reactor. Additionally, a model will be introduced to evaluate the impact on the bubble size and gas interchange coefficient in the bed.

3. MATERIALS AND METHODS

3.1. Experimental Section. A laboratory-scale 253 MA steel reactor, shown in Figure 3, was used for the experiments. The cylindrical reactor had a height of 1.27 m and an inner diameter of 78 mm. The reactor was located inside a cubic electrical furnace. There were eight measurement tubes located on both the front and back sides of the reactor wall. The tubes on the back side are used for thermocouples and pressure sensors. The tubes on the front side are used to connect gas sampling tubes. Normally, only one of the front tubes is used at each time for gas sampling. The tubes on the back side are connected at an angle of 45° with respect to the reactor body, while the front tubes are horizontal. The furnace temperature was set to achieve a reactor temperature of 840 °C, for all experiments performed. The top of the reactor is open and located in a metal fume hood. Experiments have been performed to validate that back mixing of air from the open outlet should not influence the experiments performed.

The measurement points (MPs) are located as shown in Figure 3, at heights listed in Table 1.

Table 1. Vertical Position of Measurement Tubes Relative to the Distributor Plate

MP	height (cm)	measured data
windbox		temperature and pressure
1	3.65	temperature, pressure, and gas concentration
2	8.88	temperature, pressure, and gas concentration
3	13.65	temperature, pressure, and gas concentration
4	15.65	temperature, pressure, and gas concentration
5	31.65	temperature, pressure, and gas concentration
6	47.65	temperature, pressure, and gas concentration
7	63.65	temperature, pressure, and gas concentration
8	79.65	temperature, pressure, and gas concentration

The gas distributor plate was a 5 mm thick hole plate with 61 holes, each with a diameter of 0.6 mm. To stop bed particles from falling into the windbox, a small air flow was applied to the windbox also during down time. Further, when the reactor was emptied, the wind box was opened and inspected to ensure that no particles were present and that the holes were not clogged.

Because the fuel conversion rate is the key factor that needs to be verified at the outlet of the bed, the gas samples were taken from sampling point 8 (79.65 cm above the distributer plate) for all bed heights (as shown in Figure 3). This point was chosen to ensure that the gas was not sampled from inside the bed or from the splash zone. The flue gas was sent to a gas analyzer SICK GMS810. Sampling was via a polytetrafluoroethylene (PTFE) tube heated to 190 °C, to ensure that condensation was avoided. The SICK GMS810 gas analyzer measured the composition of gas in volume percent for relevant gas components, including CO_2, CO, H_2, and O_2. The

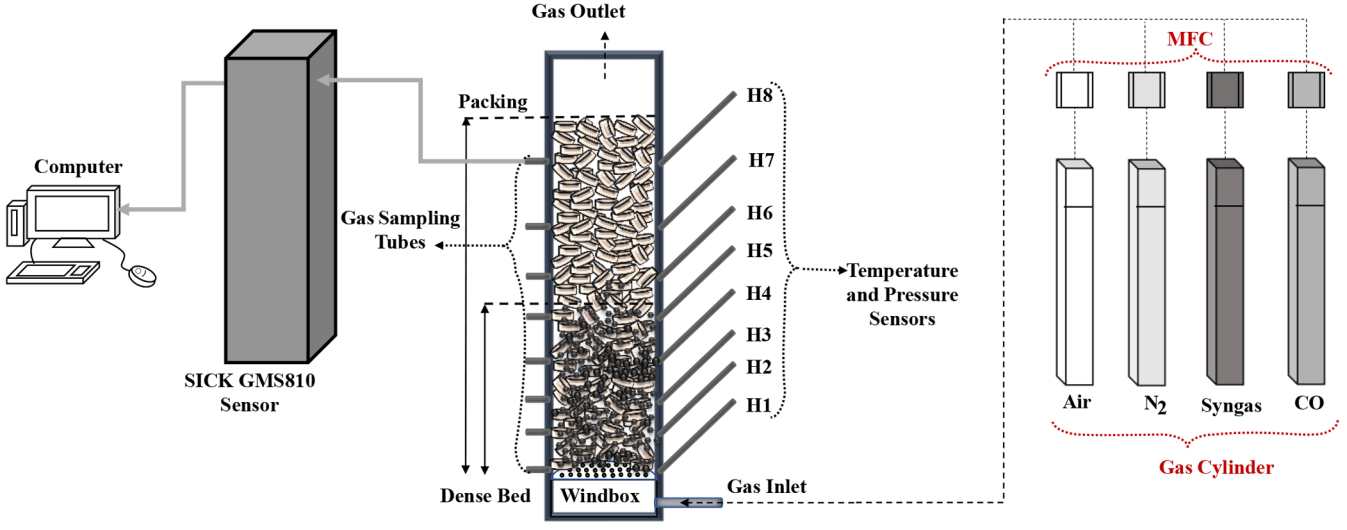

Figure 3. Schematic illustration of the reactor for batch CLC reactions.

https://doi.org/10.1021/acs.energyfuels.2c00527
Energy Fuels XXXX, XXX, XXX−XXX

temperature, pressure, and flow rate for each gas were also measured and logged. The mass balance closure accuracy on carbon is about 90% on average for the whole fuel feeding period on the basis of gas measurement data. However, the response for gas measurement is not a perfect step function, suggesting that some back mixing occurs during the first few seconds when switching from nitrogen to fuel. This is expected and not believed to influence the analysis or conclusions.

3.2. Packings and Bed Material. The packings used in the experiments were a 25 mm stainless-steel thread saddle (RMSR) and 25 mm stainless-steel pall ring (Hiflow). The nominal bulk density was 228 kg/m^3 for RMSR and 372 kg/m^3 for Hiflow. The packings have very different geometries, as seen in Figure 4.

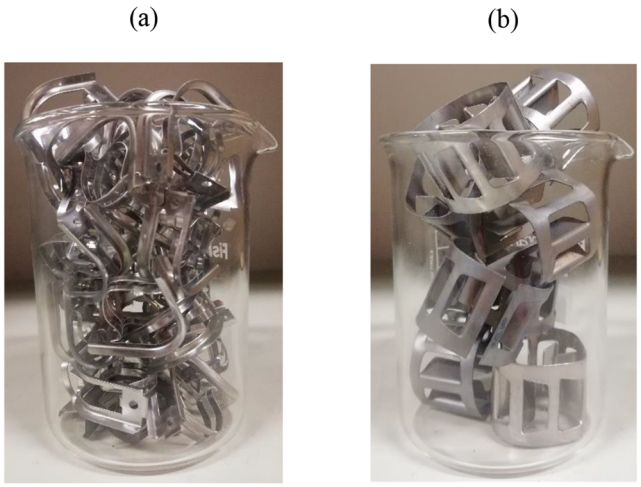

Figure 4. Packings investigated in this study: (a) RMSR and (b) Hiflow.

Packing data provided above are nominal values from the manufacturer. They represent expected values when the packings are used for industrial applications. However, the packings are quite large compared to the reactor used here. Thus, perfect packing conditions will not be achieved, and there will be a random element as to exactly what void factor is achieved. To account for this, we measured the actual bulk density of packings by pouring them into a container with a known volume and similar diameter as the reactor vessel while recording the change in mass and dividing it by the volume. The actual void factor, ε, is also needed to be determined experimentally for both types of packings because it is needed to calculate the residence time of the fuel and the amount of ilmenite required to obtain the desired bed height. To find the void factor of the packing material, an empty container was filled with water and weighed. The container was then emptied and filled with packings. Water was added to the packed container until it was completely full and weighed. Dividing the weight of the water in the packed container by the weight of the water in the unpacked container gives the void factor. It was observed that the values obtained were not totally consistent with data provided by the manufacturer. This reflects the randomness of adding these packings to a rather small vessel. The mass of packings required to fill the reactor up to 1 m were calculated by multiplying the volume of the reactor, the measured void factor, and the measured density of the packings and shown in Table 2.

Ilmenite concentrate was chosen as the bed particles and oxygen carrier. Ilmenite concentrate is the crushed and beneficiated form of the mineral ilmenite. This is an ore mined for production of TiO_2. The concentrate consists mainly of iron and titanium oxides ($FeTiO_3$, Fe_2TiO_5, Fe_2O_3, TiO_2, and Fe_3O_4). As in previous work,[20] ilmenite that had already been subject to continuous CLC operation in a small pilot reactor with liquid and gaseous fuels was used. This is to ensure that the material was at steady-state conditions; i.e., its physical properties and reactivity would be stable over the whole set of

Table 2. Measured Characteristics of RMSR and Hiflow Packings and Their Required Mass for 1 m Packing Height

	measured bulk density (kg/m^3)	nominal void factor	actual void factor	volume of reactor occupied with packing (m^3)	required mass of packing (kg)
RMSR	195	0.96	0.975	0.0048	0.932
Hiflow	271	0.95	0.965	0.0048	1.295

experiments. The bulk density of ilmenite was measured to 1637 kg/m^3. Further, the particles were sieved to the size range of 90−250 μm (Figure 5). The mean particle diameter was calculated to 179 μm, by applying eq 5.

$$\bar{d}_p = \frac{1}{\sum_i \frac{x_i}{d_{pi}}} \quad (5)$$

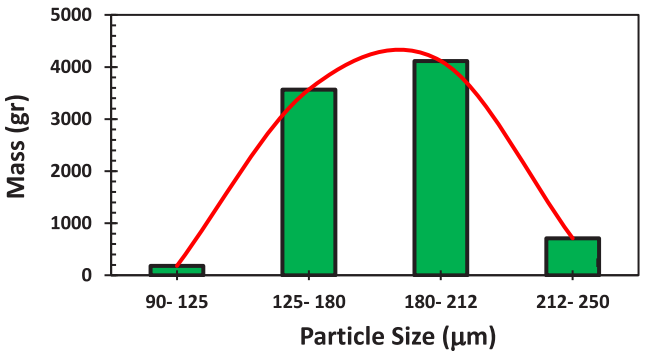

Figure 5. Particle size distribution for ilmenite particles used in this work.

3.3. Gases. Investigated fuel gases were syngas (50:50% H_2/CO) and carbon monoxide. Syngas is a representative fuel for practical applications. CO was used because it simplifies data evaluation, which could make it easier to draw firm conclusions. Nitrogen (N_2) was used as inert gas. Air was used as the oxidizing gas. The total gas flow rate of 21 L_n/min was used in the oxidation and reduction steps. The maximum flow provided by the fuel gas mass flow controller (MFC) was 15 L_n/min. Thus, 6 L_n/min of nitrogen gas was added during fuel feeding. This also ensured that there was always a minimum gas flow to the reactor during gas switching. The flow rates of gases during operation are specified in Table 3.

Table 3. Flow Rate of Gases during the Batch CLC Process

process	oxidation	inert	reduction with syngas		reduction with CO	
gas	air	N_2	syngas	N_2	CO	N_2
flow rate (L_n/min)	21	10	15	6	15	6

3.4. Experimental Procedure. For the experiments with packings, the reactor was first filled with packing up to a 1 m height. Then, in the first step, ilmenite was added to a 10 cm bed height and the air flow was set to 21 L_n/min. The next step was to set the target temperature of the reactor to 840 °C. The particles were then oxidized during heating. When the temperature was stabilized, the gas flow was changed to N_2. After excess oxygen was removed from the reactor, the mixture of fuel gas and N_2 was introduced for the duration of the calculated reaction time (as shown in Table 3). The reaction time for each experiment was set so that 0.8% reduction of ilmenite was ensured. The exact time for each measuring point is a function of the mass of bed material, fuel flow, and expected fuel conversion rate. To purge the reactor and make sure that no fuel or product were left after each step, the reactor was fluidized with N_2 gas. Finally, gas was

https://doi.org/10.1021/acs.energyfuels.2c00527
Energy Fuels XXXX, XXX, XXX−XXX

Table 4. Ilmenite Settled Bed Height, Mass, and Reaction Time Used for Syngas and CO Fuels

		packing					
		no packing		RMSR		Hiflow	
number	settled ilmenite height (cm)	ilmenite mass in bed (g)	time of reduction (s)	ilmenite mass in bed (g)	time of reduction (s)	ilmenite mass in bed (g)	time of reduction (s)
1	10	782	32	749	30	743	30
2	15	1173	48	1123	45	1114	45
3	20	1564	64	1497	60	1486	60
4	25	1955	80	1872	75	1857	75
5	30	2346	96	2246	90	2229	90
6	35	2737	112	2621	105	2600	105
7	40	3128	128	2995	120	2972	120
8	50	3910	160	3744	150	3715	150
9	55	4302	176	4118	165	4086	165
10	60	4693	192	4492	180	4458	180

set back to air to oxidize the reduced oxygen carrier particles. Each experiment was repeated at least 3 times, to ensure repeatability. The results were analyzed on the basis of the average of all measurements. The next set of experiments was performed by adding ilmenite up to the next desired bed height level and repeating the above procedure. Table 4 presents the settled bed height, ilmenite mass, and time of reaction for both syngas and CO fuels and different packings.

3.5. Experimental Evaluation. The fuel conversion rate for this study can be obtained through the chemical reactions and mass balances. The net reaction in a FR with CO fuel is given in eq 6. For the syngas as fuel, the reaction will be eq 7.

$$CO + M\_O \rightarrow CO_2 + M \tag{6}$$

$$CO + H_2 + 2M\_O \rightarrow CO_2 + H_2O + 2M \tag{7}$$

In this paper, the fuel conversion rate is presented on the basis of the gas yield, γ, which is defined for CO and syngas in eqs 8 and 9, respectively. In the case of syngas, the inlet and outlet flows of H_2 must be accounted for as water is condensed prior to the analysis. Thus, eqs 8 and 9 can be obtained from a mass balance between inlets and outlets.[22]

$$\gamma_{CO} = \frac{\dot{n}_{CO_2,out}}{\dot{n}_{CO,out} + \dot{n}_{CO_2,out}} \tag{8}$$

$$\gamma_{syngas} = \frac{\dot{n}_{CO_2,out} + \dot{n}_{H_2,in} - \dot{n}_{H_2,out}}{\dot{n}_{CO,out} + \dot{n}_{CO_2,out} + \dot{n}_{H_2,in}} \tag{9}$$

The conversion of H_2 is calculated using eq 10.[22]

$$\gamma_{H_2} = \frac{\dot{n}_{H_2,in} - \dot{n}_{H_2,out}}{\dot{n}_{H_2,in}} \tag{10}$$

Another important parameter is the mass-based conversion of the oxygen carrier, which can be obtained from eq 11.

$$X = 1 - \frac{m}{m_{ox}} \tag{11}$$

The momentary conversion of the oxygen carrier can be calculated with eq 12 for CO and with eq 13 for syngas.

$$X_i = X_{i-1} + \int_{t-1}^{t} \frac{\dot{n}M_O}{m_{ox}}(y_{CO_2})dt \tag{12}$$

$$X_i = X_{i-1} + \int_{t-1}^{t} \frac{\dot{n}M_O}{m_{ox}}(2y_{CO_2} + y_{CO} - y_{H_2})dt \tag{13}$$

In this paper, the fuel conversion, γ, is presented as the average value for an oxygen carrier conversion span in the range of $0.001 < X < 0.008$. This is to avoid the extreme apparent changes in the conversion rate at the moment when the fuel is introduced ($X < 0.001$) or when ilmenite has lost much of its available oxygen as a result of reduction ($X > 0.008$). The conversion rate is calculated as the average rate during this interval. Most of the experiments are repeated at least 3 times for each set of parameters.

3.6. Modeling. Several methods were employed to quantify the effect of the packings on the gas−solid mass transfer rate and the gas conversion in CLC. First, the effective reaction contact factor, which is the multiplication of contact efficiency and reaction rate constant for the combustion experiments, will be estimated as k_f ($Nm^3\ kg^{-1}\ s^{-1}$). This expression takes into account the effect of gas conversions, γ, on k_f.

Further, as discussed in a previous work,[20] packings will affect the reaction rate through changing the mass transfer rate between the bubble phase and the emulsion phase, which is believed to be one of the reaction bottlenecks. In other words, packings will affect the mass transfer rate by changing the surface area between bubbles and emulsion through changing the bubble size. Thus, in the next step, a model for calculating the average bubble size, d_b (m), and then the overall interchange coefficient between the bubble phase and emulsion phase, K_{be} (s^{-1}), will be introduced. For this purpose, the two-phase theory model was applied. The details will be described in section 3.6.2.

3.6.1. Reaction Contact Factor. For the reaction contact factor, a model devised by Aronsson et al.[22] and Berguerand et al.[35] was used. The proposed model calculates a mass-based first-order effective reaction contact factor, k_f ($Nm^3\ kg^{-1}\ s^{-1}$), through eq 14.

$$k_f = \eta k_r = \frac{\alpha F_0}{m} \tag{14}$$

where F_0 is the volumetric gas flow rate (Nm^3/s), m is the mass of the oxygen carrier (kg), k_r is the reaction rate constant ($Nm^3\ kg^{-1}\ s^{-1}$), and η is the contact efficiency. The dimensionless number α is in direct relation to gas conversion, γ, through eq 15.

$$\alpha = \ln\left(\frac{1}{1-\gamma}\right) \tag{15}$$

3.6.2. Gas Interchange Coefficient. In bubbles (when $u_{br} > u_{mf}/\varepsilon_{mf}$), a cloud of circulating gas envelops the bubble as it rises up through the bed according to Kunii and Levenspiel[36] (Figure 6). In the above definition, u_{br} is the rise velocity of a single bubble with respect to the emulsion phase (m/s), u_{mf} is the minimum fluidization velocity (m/s), and ε_{mf} is the void fraction in the bed at minimum fluidization. Considering the interchange of gas A from a bubble, we can define two coefficients: the interchange coefficient between the bubble and cloud, K_{bc} (s^{-1}), and the interchange coefficient between the cloud and emulsion, K_{ce} (s^{-1}).[36]

These coefficients can also be referred to as the crossflow rates. The overall coefficient between the bubble and emulsion in a bubbling bed is K_{be} (s^{-1}) and is defined in eq 16.[36]

https://doi.org/10.1021/acs.energyfuels.2c00527
Energy Fuels XXXX, XXX, XXX−XXX

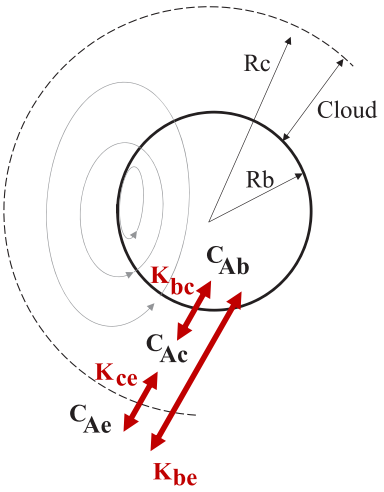

Figure 6. Gas streamlines and illustration of exchange coefficients near a single rising bubble in a clouded bubble.

$$K_{be} = \left[\frac{\text{volume of gas going from bubble to emulsion or vice versa}}{(\text{volume of bubble in the bed})(\text{time})}\right] = \frac{1}{\frac{1}{K_{bc}} + \frac{1}{K_{ce}}} \tag{16}$$

in which coefficients K_{bc} (s^{-1}) and K_{ce} (s^{-1}) are dependent upon the bubble size, d_b (m), and are calculated as[36]

$$K_{bc} = 4.5\left(\frac{u_{mf}}{d_b}\right) + 5.85\left(\frac{D^{1/2}g^{1/4}}{d_b^{5/4}}\right) \tag{17}$$

$$K_{ce} = 6.77\left(\frac{D\varepsilon_{mf}u_{br}}{d_b^{3}}\right)^{1/2} \tag{18}$$

where D (m^2/s) is the molecular diffusion coefficient of gas, u_{br} is the rise velocity of a single bubble with respect to the emulsion phase (m/s), and u_{mf} (m/s) and ε_{mf} are the superficial gas velocity and void fraction in the bed at minimum fluidizing conditions. The diffusion coefficient of CO, D_{CO}, in air at atmospheric pressure is linearly dependent upon the temperature.[37] Thus, D_{CO} was estimated as 1.799 cm^2/s at 840 °C for this work (more information is provided in the Supporting Information).

Nemati et al.[38] suggested eq 19 to calculate the void fraction in a fluidized bed, ε_f, as a function of the standard deviation of pressure fluctuations, σ (Pa).

$$\varepsilon_f = 1.5\left(\frac{\sigma}{0.438\rho_p g L}\right)^{0.8896} \mathrm{Ar}^{-0.0211}\left(\frac{L}{D_c}\right)^{-0.388} \tag{19}$$

When considering a bubbling bed as a two-phase system, it is assumed that all gas in the excess of u_{mf} (m/s) flows through the bed as bubbles, while the emulsion stays stagnant at minimum fluidizing conditions (Figure 7). The average bed voidage, ε_f, then becomes related to the fraction of the bed in bubbles, δ, and the voidage of the emulsion, ε_e, by eq 20.

$$\varepsilon_f = \delta + (1 - \delta)\varepsilon_e \tag{20}$$

For the two-phase theory model, as mentioned, emulsion stays at minimum fluidizing conditions. Thus, ε_e can be estimated as eq 21 for Geldart B solids.

$$\varepsilon_e = \varepsilon_{mf} \tag{21}$$

The fraction of bed in bubbles will be calculated as

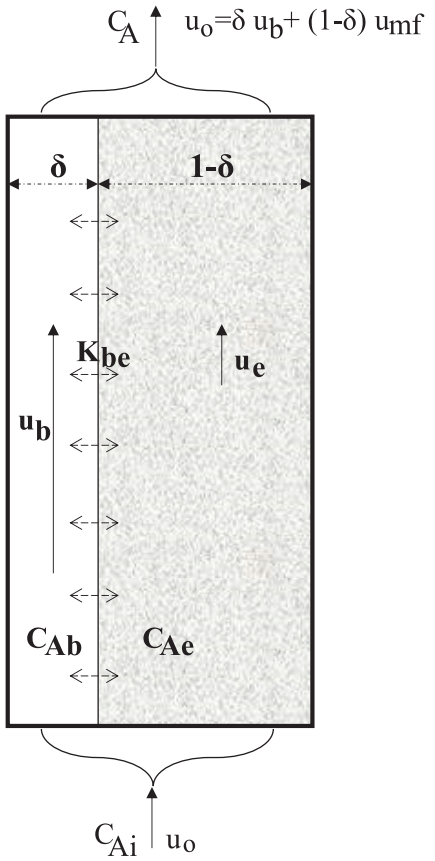

Figure 7. Two-phase theory model.

$$\delta = 1 - \frac{1 - \varepsilon_f}{1 - \varepsilon_{mf}} \tag{22}$$

On the other hand, the bed fraction in the bubbles is related to the bubble diameter, d_b (m), as in eqs 23 and 24 in the two-phase model.[36]

$$\delta = \frac{u_o - u_{mf}}{u_b - u_{mf}} \tag{23}$$

In eq 24, the rise velocity of bubbles, u_b (m/s), is the same as the rise velocity of a single bubble, u_{br} (m/s), and calculated as

$$u_b = u_{br} = 0.711(gd_b)^{1/2} \tag{24}$$

Eliminating δ in eqs 22, 23, and 24 gives the relationship between ε_f and d_b (m) as

$$\frac{\varepsilon_f - \varepsilon_{mf}}{1 - \varepsilon_{mf}} = \frac{u_o - u_{mf}}{0.711(gd_b)^{1/2} - u_{mf}} \tag{25}$$

or

$$d_b = \frac{1}{(0.711)^2 g}\left[u_{mf} + (u_o - u_{mf})\frac{1 - \varepsilon_{mf}}{\varepsilon_f - \varepsilon_{mf}}\right]^2 \tag{26}$$

In this study, u_{mf} (m/s) and ε_{mf} are considered the same for all cases with and without packing. This was investigated through other experiments for RMSR packing with a void factor of 0.96. Thus, u_{mf} (m/s) was calculated with the equation proposed by Chitester et al.[36] for the coarse particles as

https://doi.org/10.1021/acs.energyfuels.2c00527
Energy Fuels XXXX, XXX, XXX−XXX

$$\frac{d_p u_{mf} \rho_g}{\mu} = \left[(28.7)^2 + 0.0494 \left(\frac{d_p^3 \rho_g (\rho_s - \rho_g) g}{\mu^2} \right) \right]^{1/2} - 28.7 \quad (27)$$

where u_{mf} (m/s) depends upon the bed temperature. As the bed temperature increases, the minimum fluidization velocity decreases as a result of the decreasing fluidizing gas density and increasing gas viscosity. For packed fluidized beds, similar tendencies can also be expected. ε_{mf} was calculated using eq 28[36]

$$\frac{1.75}{\varepsilon_{mf}^3 \varphi_s} \left(\frac{\rho_p u_{mf} d_p}{\mu_g} \right)^2 + \frac{150(1 - \varepsilon_{mf})}{\varepsilon_{mf}^3 \varphi_s^2} \left(\frac{\rho_p u_{mf} d_p}{\mu_g} \right) = \mathrm{Ar} \quad (28)$$

where φ_s is the sphericity of the particles and was assumed to be 0.67, which is a typical value for sharp sands according to Kunii and Levenspiel.[36]

4. RESULTS

4.1. Average Fuel Conversion as a Function of the Bed Height. Figure 8 shows the average fuel conversion for syngas for bed heights ranging from 10 to 60 cm, when using RMSR and Hiflow packing, and for a bubbling bed with no packing. A typical concentration profile of outlet gas concentrations for one cycle can be found in Figures S1−S4 in the Supporting Information.

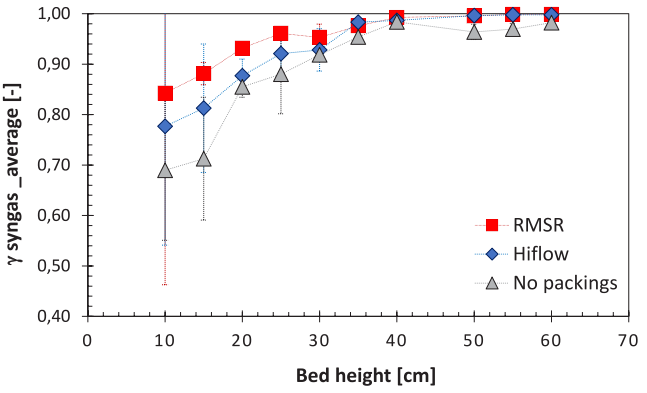

Figure 8. Average syngas conversion as a function of the bed height: syngas at 15 L_n/min, N_2 at 6 L_n/min, and temperature of 840 °C.

Figure 9 shows average fuel conversion for CO as fuel for bed heights ranging from 10 to 60 cm, using RMSR, Hiflow, and bed with no packing. The conversion rates for both syngas and CO fuels are calculated by the measured data at a temperature of 840 °C and the measurement point MP8. The standard deviation bars are calculated by comparing at least three experiments being conducted at each set of conditions. In both Figures 8 and 9, the fuel conversion was represented by the average value for X in the interval of 0.001−0.008.

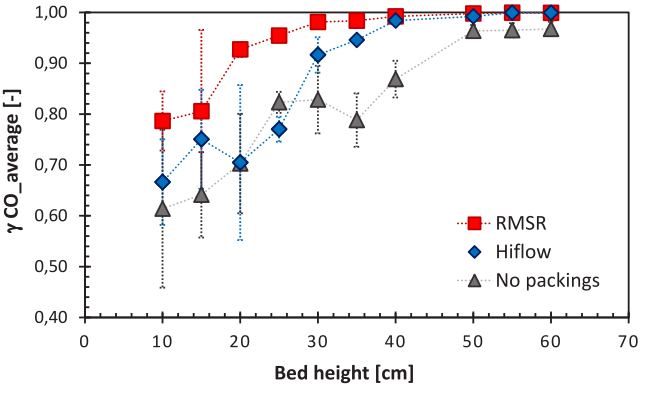

Figure 9. Average CO conversion as a function of the bed height: CO at 15 L_n/min, N_2 at 6 L_n/min, and temperature of 840 °C.

Figures 8 and 9 show that the fuel conversion generally increases with increasing bed heights. This is expected and represents increased opportunities for the fuel to react with the oxygen carrier by the increased residence time of gas in the bed. The improvement is most pronounced when going from relatively shallow beds to slightly less shallow beds (e.g., from 10 to 20 cm). For the deeper beds (above 50 cm), fuel conversion is relatively stable or changes only slightly. This is also expected. First, as fuel conversion increases, the driving force for further conversion is reduced. This means that it is much less difficult to improve fuel conversion from, e.g., 60 to 70%, as compared to increasing it from 90 to 100%. Second, for Geldart group B particles, bubbles will grow as a function of the bed depth. Larger bubbles are expected to result in reduced mass transfer from gas to solids. The second factor, i.e., the changes in mass transfer as a result of bubble growth, coalescence, and eruption, should be more pronounced in beds with no packing. In the packed fluidized beds, the packing should limit bubble growth. Interestingly, essentially full conversion of syngas and CO is achieved already at 40 cm bed height for packed fluidized beds. For the unpacked bed, fuel conversion is limited to about 95% and increasing the bed height above 50 cm has only a marginal effect. Finally, it is mentioned that, for gaseous and liquid flows, packings are known to influence flow characteristics, in such a way that lower Reynolds numbers are required to achieve turbulent flow. It is not known if or how such observations will translate to packed fluidized beds. However, potentially, this could be another mechanism that would affect mass transfer that could not be explained by changes in the bubble size.

In Figures 8 and 9, it can be seen that the trend with respect to fuel conversion in relation to the bed height is similar for syngas and CO (more information provided in Figures S5−S7 of the Supporing Information). For bed heights between 10 and 30 cm, the fuel conversion with RMSR is more than 10% higher than experiments using Hiflow packings and more than 20% higher than without packings. For example, Figure 8 shows that RMSR improves the fuel conversion for syngas from 0.84 (for 10 cm bed height) to 1 (for 60 cm bed height), which is a significant improvement in comparison to the bed with no packings (from 0.69 up to 0.98). Figures 8 and 9 also indicate that the fuel conversion is similar for both packing types when the bed height reaches or exceeds 40 cm. At those heights, nearly 100% conversion is achieved with both packings. For all evaluated bed heights, fuel conversion remained lower in a bubbling bed without packings than in beds with packings. In general, the highest conversion rates are achieved during experiments using RMSR packings.

Hiflow packings were also successful to increase fuel conversion (up to ≅1). However, RMSR showed better improvements for the whole range of bed heights in the experiments. The same trends are observed in Figure 9 for CO as the fuel gas. The main reason for improvements in the conversion with packings can be attributed to the ability of packings to increase the mass transfer rate, presumably by breaking down bubbles. This conclusion will be further discussed below.

https://doi.org/10.1021/acs.energyfuels.2c00527
Energy Fuels XXXX, XXX, XXX−XXX

It is noted that there are two odd data points. Seemingly, there is a decrease in fuel conversion at 20 cm bed height for Hiflow packing as well as 35 cm for the bed with no packing in Figure 9. For the bed with Hiflow packings, this effect may be due to the packing by chance, arranging themselves in some unfavorable pattern. Random packings will not necessarily pack perfectly in a reactor. The packings used here are the smallest size available for industrial applications, but they are very large compared to what would be ideal for the lab reactor used. While RMSR and Hiflow are nominally of the same size, Hiflow is clearly much bulkier and packs less readily in the small reactors used. It is conceivable that this could be the reason behind the unexpected results for some arrangements.[20,28] For the odd point in the unpacked bed, it could be argued that it is within the natural variation expected for the reactor, judging by the standard deviation error bars.

4.2. Average Fuel Conversion as a Function of the Pressure Drop. The average conversions of syngas and CO as a function of the bed pressure drop are plotted in Figures 10 and 11. In these figures, the pressure drop of the bed is calculated from the atmospheric pressure, the pressure in the windbox, and the pressure drop over the distributor plate.

$$\Delta P_{bed} = P_{WB} - \Delta P_{distributor} - P_{atm} \quad (29)$$

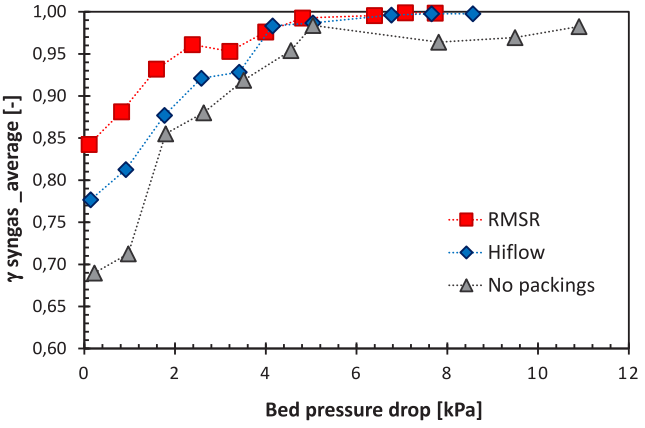

Figure 10. Average syngas conversion as a function of the bed pressure drop: syngas at 15 L_n/min, N_2 at 6 L_n/min, and temperature of 840 °C.

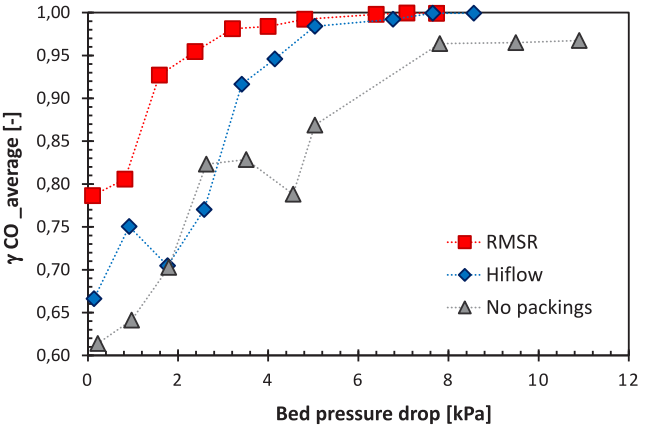

Figure 11. Average CO conversion as a function of the bed pressure drop: CO at 15 L_n/min, N_2 at 6 L_n/min, and temperature of 840 °C.

When the fuel conversion is plotted as a function of the pressure drop, as in Figure 10 and 11, a clear improvement of the fuel conversions can be seen for cases when packings are used. For example, in Figure 10, for 97% syngas fuel conversion, the pressure drop with RMSR and Hiflow packing is around 4 kPa, while more than 7 kPa is needed for the same gas conversion for beds with no packing. Figure 11 shows that, for 97% CO conversion, the pressure drop with RMSR packing is around 3.2 kPa and with Hiflow packing is 5 kPa, while it increases to more than 9.5 kPa for beds with no packing. These are very significant improvements and would greatly influence reactor design.

4.3. Reaction Contact Factor and Gas Interchange Coefficient. Figures 12−14 present some raw data of pressure signals (kPa) as a function of time (s), for different bed heights from 10 to 40 cm. The data in Figures 12−14 are gathered for one complete redox cycle (as shown in Table 3). A slight decrease in the pressure fluctuations in the time interval of 100−400 s can be observed, especially for the cases in Figure 12. This is due to a lower flow rate in the inert step (10 L_n/min) compared to the other steps of the cycle (21 L_n/min). All data presented in Figures 12−14 are measured at point MP1, 3.65 cm over the distributor plate, and for syngas as fuel. The results for CO are similar to syngas. Thus, they have not been included in the figures. As shown in Figures 12−14, the pressure measurements clearly show that the experiments without packing have a higher peak amplitude and generally larger pressure fluctuations compared to experiments using

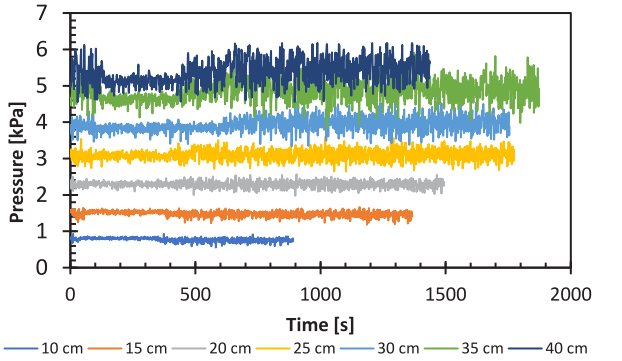

Figure 12. Raw data of pressure signals for one cycle for beds with no packing as a function of time: syngas as fuel, temperature of 840 °C, and pressure data gathered at MP1 using a measurement frequency of 1 Hz.

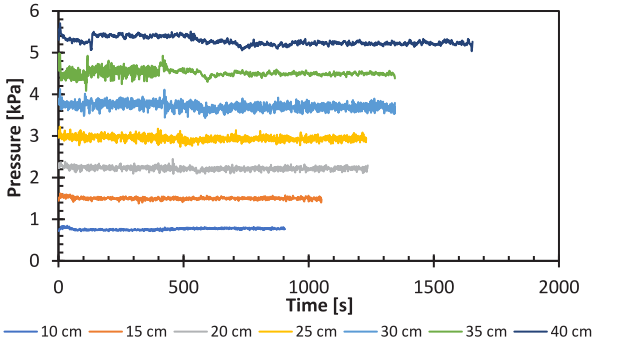

Figure 13. Raw data of pressure signals for one cycle for RMSR as a function of time: syngas as fuel, temperature of 840 °C, and pressure data gathered at MP1 using a measurement frequency of 1 Hz.

https://doi.org/10.1021/acs.energyfuels.2c00527
Energy Fuels XXXX, XXX, XXX−XXX

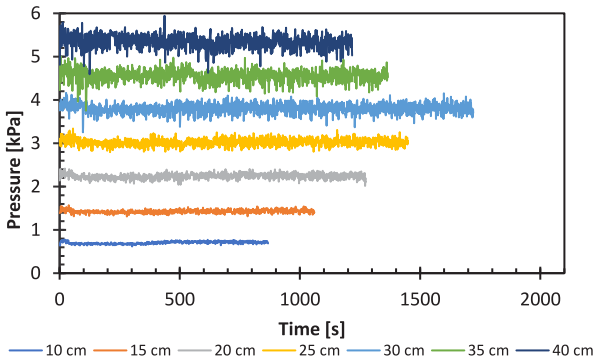

Figure 14. Raw data of pressure signals for one cycle for Hiflow as a function of time: syngas as fuel, temperature of 840 °C, and pressure data gathered at MP1 using a measurement frequency of 1 Hz.

packings. Figure 13 shows that RMSR provides the most stable pressure over time.

The average bubble diameter was calculated with eq 26 in the previous section, and the results are shown in Figure 15.

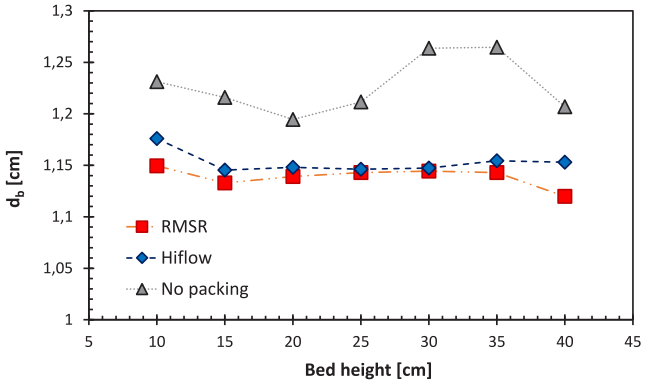

Figure 15. Changes of the bubble diameter as a function of the bed height, as estimated by eq 26, with pressure data gathered and analyzed at MP1 using a measurement frequency of 1 Hz.

Data were gathered at MP1, located at 3.65 cm above the distributor plate. This measurement point was chosen to ensure that, for all bed heights, the pressure sensor is located inside the bed. Thus, the signals will be related to bubble formation, coalescence, eruption, etc. in the packed fluidized bed and not in the splash zone. The results can be assumed to represent an estimation of an average value. It should be mentioned that, for bed heights over 40 cm, the pressure sensor was occasionally reaching its maximum amplitude. Thus, variance in recorded pressure fluctuations could not be used to estimate the bubble diameter for these bed heights. Therefore, they are not shown in Figure 15.

Figure 15 illustrates that the bubble diameter in packed beds containing high void packings of RMSR and Hiflow are very close to each other and around 8% less than beds without packings. Thus, the surface area where gas enters or exits the bubble decreases by 17%, and the gas volume in each bubble decreases by 25%. This ability of packings in reducing the bubble size can be assumed to contribute to the improvement in fuel conversion observed in Figures 8 and 9. When small bubbles are prevented from growing to bigger bubbles by applying packings, the boundary area between the bubble phase and the emulsion phase will increase. As a result of increasing the boundary area, the mass transfer will improve.

Ultimately, the fuel conversion will be decided mainly by the bottlenecks in the whole fuel conversion chain (transport of reactants to the particle surface, reaction between gas and particle, oxygen transfer within the particle, removal of products from the surface, etc.). It is important to point out that the gas−solid mass transfer, both to and from the particle surface, is the only parameter factor that is altered by applying packings. This is performed by increasing the surface area between bubbles and the emulsion, as described above. Thus, the fact that packings improve fuel conversion suggests that gas−solid mass transfer indeed is a significant bottleneck in the fuel conversion chain, at least for the specific situation examined in this study.

When applying packings, the conversion rate will increase, as shown in Figures 8 and 9. To better illustrate the effect of packings, reaction contact factor, k_f ($Nm^3\ kg^{-1}\ s^{-1}$), and gas interchange coefficient, K_{be} (s^{-1}), are depicted in Figures 16 and 17 as a function of the bed height, respectively.

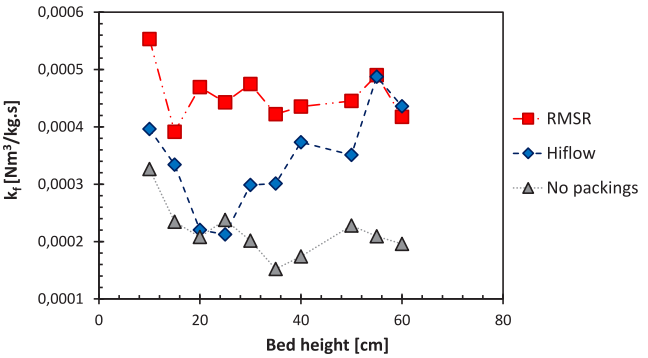

Figure 16. Changes of k_f as calculated by eq 14 as a function of the bed height, with pressure data gathered and analyzed at MP1.

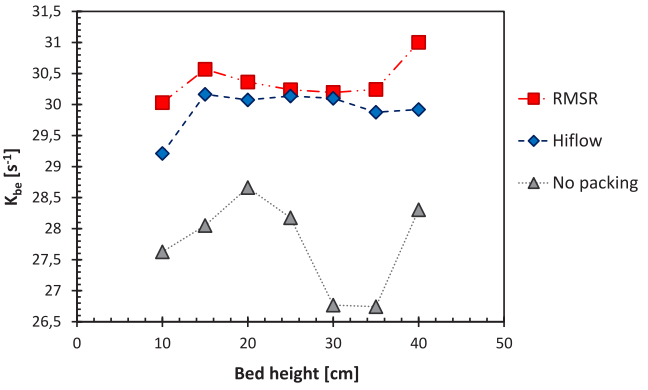

Figure 17. Changes of K_{be} as calculated by eq 16 as a function of the bed height, with pressure data gathered and analyzed at MP1.

Figure 18 shows the variation of k_f as a function of K_{be}. As illustrated in Figure 18, applying RMSR and Hiflow packings will improve both K_{be} and k_f in the system compared to the bed with no packings. This improvement is more significant for RMSR packing. As mentioned in the previous sections, the void factor of both packings is quite similar to each other (more than 95%). This difference in results is probably related to the geometry of packings and how well it stacks in the current reactor. The RMSR packing, as a result of its geometry, clearly fits more effortlessly. Also, the Hiflow packings are bulkier and can be expected to suffer from more significant wall

https://doi.org/10.1021/acs.energyfuels.2c00527
Energy Fuels XXXX, XXX, XXX−XXX

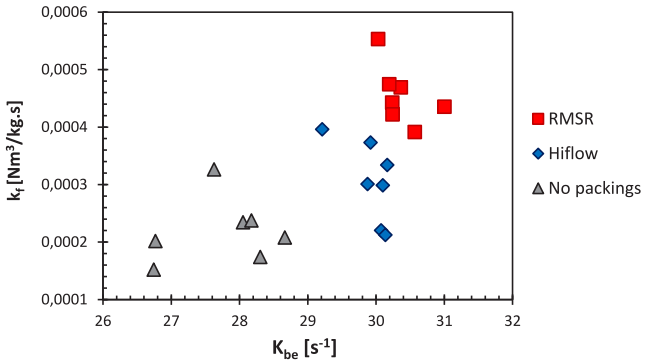

Figure 18. Changes of k_f as a function of K_{be}, with pressure data gathered and analyzed at MP1.

effects. This trend was also confirmed in the other work where the heat transfer in the packed fluidized beds was investigated.[28,39] Results indicate that the inhibition of large bubbles in the RMSR packed fluidized bed reactor increases the average K_{be} and thus the mass transfer rate (up to 9%) (Figure 17). Hence, average k_f or the fuel contact factor (up to 109%) (Figure 16) was compared to beds with no packing. These improvements are 7.7 and 57% for Hiflow packings compared to a bed with no packing, respectively.

5. DISCUSSION

The use of a packed fluidized bed as a method to improve mass transfer between bubbles and the emulsion phase and gas−solid mass transfer has been investigated. Using a combination of experimental and modeling approaches, it is shown that the mass transfer of gas between different phases can be enhanced considerably using packings. This can have implications for many fluidized bed technologies, and here, the focus was on chemical looping. It was confirmed that packings increased the fuel conversion for all bed heights and amounts of ilmenite assessed. Figures 8 and 9 contain the fuel conversions for experiments with syngas and CO fuel, using RMSR, Hiflow, and no packings and bed heights from 10 to 60 cm. A general trend is that the fuel conversion increases with increasing bed height. Beyond 40 cm bed height with RMSR or Hiflow packings, the fuel conversion is approaching 100%. At lower bed heights, effects from large bubbles or slugging are unlikely to be a factor because there is not sufficient time for small bubbles to coalesce. Because a constant bed height leads to an increased fuel conversion when combined with packings, it can be concluded that packings do provide significant benefits when applied to a bubbling CLC FR. When the results from experiments using RMSR, Hiflow, or no packings are compared, RMSR stands out as having the highest overall fuel conversion, regardless of bed height or fuel type.

The fuel conversion in relation to the pressure drop can be seen in Figures 10 and 11. In comparison of the results with and without packings, the pressure drop is consistently lower when they are present, a result that is in agreement with earlier studies.[20] The pressure drop is caused by particle hold up, friction between the packings and gas, and friction between bed particles and the packings. For the experiments without packings, because there are no other known factors involved, the observed pressure drop is believed to be due to particle hold up. The presence of packings will reduce the pressure drop in the bed for a similar fuel conversion compared to beds with no packing.

A previous study suggested that the increases in fuel conversion might be due to an improvement of the mass transfer rate through the inhibition of formation of large bubbles.[20] In accordance with Figures 12−18, the size of bubbles affects the mass transfer rates and, hence, the reaction rate. As shown in Figure 15, larger bubbles are formed in beds with no packing. This will lead to less surface area between bubbles and the emulsion phase, which will eliminate the fuel conversion. Applying packings can break down the large bubbles to smaller bubbles and improve the gas interchange coefficient and the mass transfer rate, which is one of the bottlenecks for the reactions to occur (Figures 17 and 18). As a result, the reaction contact factor will improve in beds containing packings (Figure 16).

It is possible that the difference between RMSR and Hiflow packings comes from their geometries. Experimental results observed in Figure 15 point to RMSR having a more suitable geometry for bubble eliminations. RMSR has a shape that possibly would allow for a tighter lattice structure compared to the more symmetrically shaped Hiflow packings. A tighter lattice structure might be preferable in terms of bubble growth inhibition. Alternatively, it can be hypothesized that the bulkier Hiflow packings will distribute less well in the relatively small reactor vessel used here. This may result in unfavorable flow phenomena, such as bypass flow near the reactor wall. However, this cannot be easily observed in the steel reactor used. The trend observed in this study is in good accordance with the previous investigations on RMSR and Hiflow packings.[20,28,39] Ultimately, the fuel conversion rates are roughly equal for RMSR and Hiflow packings at the higher bed heights, i.e., above 40 cm. Thus, it can be concluded that, for scaled-up conditions, in which larger reactor diameters and beds deeper than 40 cm can be expected to be used, both packings could provide similar improvements.

5.1. Potential Source of Error.

In the calculations regarding the bubble diameter, d_b, and gas interchange coefficient, K_{be}, it was assumed that minimum fluidization conditions, u_{mf} and ε_{mf}, are similar for all cases, including packings and beds without packing. This assumption was made because no published results were available for the studied packings. We believe that this assumption should not affect the final results. However, it is a good idea to determine these characteristics experimentally as well. These types of experiments were out of the scope of this study but may be considered for future studies.

Another source of error could possibly be oxygen-carrying effects of the packings. However, experiments with only packings and fuel gases without a oxygen carrier showed that packings did not exhibit any oxygen-carrying effect, at the process conditions used.

Finally, there are some occasionally non-monotonic trends in Figures 9 and 11. It seems reasonable to believe that this could have been due to experimental factors. Unfortunately, it is difficult to pinpoint the exact causes. The following points should be considered: (1) The use of random packings adds certain uncertainties. This is because random packings pack randomly. In fluidization, gas will find the way of least resistance, and if the packings end up in unfavorable positions, it may influence performance in unpredictable ways. (2) In this context, it should be pointed out that the packings used (the smallest commercial size available) are very big compared to the reactor diameter. In fact, only three individual packing elements could cover the reactor cross section. Thus,

https://doi.org/10.1021/acs.energyfuels.2c00527
Energy Fuels XXXX, XXX, XXX−XXX

unpredictable packing patterns are to be expected. (3) Because the packings organize themselves randomly, conditions may alter between different experiments and different bed heights. There is no way to verify how good the packings are distributed in a hot steel reactor. (4) In principle, we would expect errors (or differences in measurements) to be larger with a low bed height, where we may have only 3−4 layers of packing rather than when we have deeper beds. This also seems to be the case. In previous work, we have observed that, with bed depths lower than approximately 15 cm, the effect of adding packings was not clear. For low bed heights, this means that the packing depth is only a few layers, which may be insufficient to achieve an even flow profile. Also, bubble size could be expected to be small with a low bed height, leaving limited space for improvement. See the previous work.[20]

6. CONCLUSION

This study investigates the possibility to improve fuel conversion in CLC by applying random metal packings in a batch fluidized bed reactor at 840 °C. The examined variables were bed height (from 10 to 60 cm), fuel type (syngas and CO), and packing type (RMSR, Hiflow, or bubbling bed with no packings). The conclusions are as follows: (1) The key finding was that the use of packings resulted in an increased fuel conversion for all evaluated bed heights, pressure drops, and amounts of bed particles. Almost full fuel conversion was achieved in a packed fluidized bed at 840 °C with a bed height of 40 cm or higher. For an unpacked bed, fuel conversion at the same conditions was in the order of 95−96%. (2) A comparison between Hiflow and RMSR packings indicates that the latter most often is better for the given circumstances. Still, both packings provided significant improvements compared to the bubbling bed with no packings. For deeper beds, the improvement was similar for both investigated packing types. (3) The fuel conversions generally increased with the bed height, which is expected as a result of longer residence for given flows. (4) Packed fluidized beds containing RMSR packings (estimated bubble diameter in the range of 1.11−1.14 cm) seem to provide better bubble inhibition compared to Hiflow (estimated bubble diameter in the range of 1.14−1.17 cm), possibly because its geometry may allow it to form a tighter lattice structure. However, the effect could also be due to a better distribution of RMSR packing over the whole cross section and less bypass flow near the reactor wall. (5) Bubble diameters in packed beds with RMSR or Hiflow packings are around 8% less than beds without packings. Thus, the surface area where gas enters or exits the bubble decreases by 17%, and the gas volume in each bubble decreases by 25%. (6) Results indicated that the inhibition of large bubbles in the RMSR packed fluidized bed reactor increases the mass transfer rate (up to 9%). The mass-based first-order effective reaction contact factor, k_p, improves up to 109% in the bed with RMSR packing compared to the bed without packings. (7) When the fuel conversion is plotted in terms of the pressure drop, an improvement of the fuel conversions can be seen when packings are used. The addition of packings can reduce the pressure drop across the bed for every fuel conversion level.

ASSOCIATED CONTENT

Supporting Information

The Supporting Information is available free of charge at https://pubs.acs.org/doi/10.1021/acs.energyfuels.2c00527.

Four samples of the raw data collected from the gas analyzer SICK GMS810, with data provided for both fuel gases, including syngas (50:50% H_2/CO) and CO for beds with no packing and beds with RMSR packings (Figures S1−S4), average CO and H_2 conversion as a function of the bed height for syngas as fuel (Figures S5 and S6), average CO conversion in syngas and CO as fuels (Figure S7), and D_{CO} (cm^2/s) in air, used in eq 17, at atmospheric pressure and different temperatures (Table S1) (PDF)

AUTHOR INFORMATION

Corresponding Author

Nasrin Nemati − *Division of Energy Technology, Department of Space, Earth and Environment, Chalmers University of Technology, Göteborg 412 96, Sweden;* orcid.org/0000-0001-7860-2034; Email: nasrinn@chalmers.se

Authors

Yukari Tsuji − *Division of Energy Technology, Department of Space, Earth and Environment, Chalmers University of Technology, Göteborg 412 96, Sweden*

Tobias Mattisson − *Division of Energy Technology, Department of Space, Earth and Environment, Chalmers University of Technology, Göteborg 412 96, Sweden;* orcid.org/0000-0003-3942-7434

Magnus Rydén − *Division of Energy Technology, Department of Space, Earth and Environment, Chalmers University of Technology, Göteborg 412 96, Sweden*

Complete contact information is available at: https://pubs.acs.org/10.1021/acs.energyfuels.2c00527

Notes

The authors declare no competing financial interest.

ACKNOWLEDGMENTS

This work has been supported by the Swedish Energy Agency (Project 46525-1—The Application of Confined Fluidization in Energy Conversion).

NOMENCLATURE

Ar = Archimedes number
C_{Ai} = component A concentration at the entrance of the column (mol/m^3)
C_A = component A concentration at the exit of the column (mol/m^3)
C_{Ab} = component A concentration in the bubble phase (mol/m^3)
C_{Ac} = component A concentration in the cloud (mol/m^3)
C_{Ae} = component A concentration in the emulsion phase (mol/m^3)
D = molecular diffusion coefficient of gas (m^2/s)
D_{CO} = molecular diffusion coefficient of CO in air (m^2/s)
D_c = column diameter (m)
d_b = bubble diameter (m)
d_P = particle diameter (m)
F_o = volumetric fuel gas flow at 20 °C and 1 atm (Nm^3/s)
g = gravitational acceleration (m/s^2)
K_{eq} = equilibrium constant
K_{bc} = interchange coefficient between the bubble and cloud (s^{-1})

https://doi.org/10.1021/acs.energyfuels.2c00527
Energy Fuels XXXX, XXX, XXX−XXX

K_{ce} = interchange coefficient between the cloud and emulsion (s^{-1})
K_{be} = overall interchange coefficient between the bubble and emulsion (s^{-1})
k_f = mass-based effective reaction contact factor ($Nm^3\ kg^{-1}\ s^{-1}$)
k_r = reaction rate constant ($Nm^3\ kg^{-1}\ s^{-1}$)
i = component i
L = initial height of the particle column (m)
m = momentary mass of the oxygen carrier (kg)
M_o = molar mass of oxygen (kg/mol)
m_{ox} = mass of the oxygen carrier in its fully oxidized form (kg)
$\dot{n}$ = total molar flow rate at the reactor outlet (mol/s)
$\dot{n}_i$ = molar flow rate of component i (mol/s)
P_{atm} = atmospheric pressure (Pa)
P_{WB} = pressure in the windbox (Pa)
t = time (s)
u_o = superficial gas velocity measured on an empty vessel basis (m/s)
u_b = rise velocity of bubbles in the fluidized bed (m/s)
u_{br} = rise velocity of a single bubble with respect to the emulsion phase (m/s)
u_{mf} = superficial gas velocity at minimum fluidization (m/s)
X = mass-based degree of conversion of the oxygen carrier
y_i = outlet volume fraction of gas component i

Greek Letters

α = dimensionless number in the reaction rate constant
δ = fraction of the bed in bubbles
ΔP_{bed} = pressure drop of the bed (Pa)
$\Delta P_{distributor}$ = pressure drop over the distributor plate (Pa)
ε_e = voidage of the emulsion
ε_{mf} = void fraction in the bed at the minimum fluidization velocity
ε_f = average void fraction in the fluidized bed
μ = gas viscosity (Pa s)
ρ_g = gas density (kg/m^3)
ρ_p = particle density (kg/m^3)
γ = fuel gas conversion
η = contact efficiency
ω = degree of oxygen carrier reduction
σ = standard deviation of pressure fluctuations (Pa)
φ_s = sphericity of particles

REFERENCES

(1) Intergovernmental Panel on Climate Change (IPCC). Implications of carbon dioxide capture and storage for greenhouse gas inventories and accounting. *IPCC Special Report on Carbon Dioxide Capture and Storage*; IPCC: Geneva, Switzerland, 2018; Chapter 9, https://www.ipcc.ch/site/assets/uploads/2018/03/srccs_chapter9-1.pdf (accessed March 28, 2022).

(2) Rueda, O.; Mogollón, J. M.; Tukker, A.; Scherer, L. Negative-emissions technology portfolios to meet the 1.5 °C target. *Global Environ. Change* **2021**, *67*, 102238.

(3) Kraxner, F.; Nilsson, S.; Obersteiner, M. Negative emissions from BioEnergy use, carbon capture and sequestration (BECS)—The case of biomass production by sustainable forest management from semi-natural temperate forests. *Biomass Bioenergy* **2003**, *24* (4), 285–296.

(4) Read, P.; Lermit, J. Bio-energy with carbon storage (BECS): A sequential decision approach to the threat of abrupt climate change. *Energy* **2005**, *30* (14), 2654–2671.

(5) Fajardy, M.; Mac Dowell, N. Can BECCS deliver sustainable and resource efficient negative emissions? *Energy Environ. Sci.* **2017**, *10* (6), 1389–1426.

(6) Bui, M.; Adjiman, C. S.; Bardow, A.; Anthony, E. J.; Boston, A.; Brown, S.; Fennell, P. S.; Fuss, S.; Galindo, A.; Hackett, L. A.; Hallett, J. P.; Herzog, H. J.; Jackson, G.; Kemper, J.; Krevor, S.; Maitland, G. C.; Matuszewski, M.; Metcalfe, I. S.; Petit, C.; Puxty, G.; Reimer, J.; Reiner, D. M.; Rubin, E. S.; Scott, S. A.; Shah, N.; Smit, B.; Trusler, J. P. M.; Webley, P.; Wilcox, J.; Mac Dowell, N. Carbon capture and storage (CCS): The way forward. *Energy Environ. Sci.* **2018**, *11*, 1062–1176.

(7) Al-Fattah, S. M.; Barghouty, M. F.; Bureau, G.; Dabbousi, B. O.; Fillacier, S.; Le Thiez, P.; McQuale, C.; Munier, G.; Royer-Adnot, J. *Carbon Capture and Storage: Technologies, Policies, Economics, and Implementation Strategies*, 1st ed.; Taylor & Francis Group: Milton Park, U.K., 2011.

(8) Lyngfelt, A.; Linderholm, C. Chemical-Looping Combustion of Solid Fuels—Status and Recent Progress. *Energy Procedia* **2017**, *114*, 371–386.

(9) Lyngfelt, A.; Brink, A.; Langørgen, Ø.; Mattisson, T.; Rydén, M.; Linderholm, C. 11,000 h of chemical-looping combustion operation—Where are we and where do we want to go? *Int. J. Greenhouse Gas Control* **2019**, *88*, 38–56.

(10) Mei, D.; Mendiara, T.; Abad, A.; de Diego, L. F.; Garcia-Labiano, F.; Gayán, P.; Adánez, J.; Zhao, H. Evaluation of Manganese Minerals for Chemical Looping Combustion. *Energy Fuels* **2015**, *29* (10), 6605–6615.

(11) Mendiara, T.; Gayán, P.; García-Labiano, F.; de Diego, L. F.; Pérez-Astray, A.; Izquierdo, M. T.; Abad, A.; Adánez, J. Chemical Looping Combustion of Biomass: An Approach to BECCS. *Energy Procedia* **2017**, *114*, 6021–6029.

(12) Tong, A.; Bayham, S.; Kathe, M. V.; Zeng, L.; Luo, S.; Fan, L. S. Iron-based syngas chemical looping process and coal-direct chemical looping process development at Ohio State University. *Appl. Energy* **2014**, *113*, 1836–1845.

(13) Lyngfelt, A. Chemical Looping combustion (CLC). *Fluidized Bed Technologies for near-Zero Emission Combustion and Gasification*; Woodhead Publishing, Ltd.: Cambridge, U.K., 2013; Chapter 20, pp 895–930, DOI: 10.1533/9780857098801.4.895.

(14) Lyngfelt, A.; Leckner, B. A 1000 MW_{th} boiler for chemical-looping combustion of solid fuels—Discussion of design and costs. *Appl. Energy* **2015**, *157*, 475–487.

(15) Mattisson, T.; Lyngfelt, A.; Leion, H. Chemical-looping with oxygen uncoupling for combustion of solid fuels. *Int. J. Greenhouse Gas Control* **2009**, *3* (1), 11–19.

(16) Abulgasim, S.; Wang, W.; Abdalazeez, A. A Brief Review for Chemical Looping Combustion as a Promising CO_2 Capture Technology: Fundamentals and Progress. *Sci. Total Environ.* **2021**, *764*, 142892.

(17) Czakiert, T.; Krzywanski, J.; Zylka, A.; Nowak, W. Chemical Looping Combustion: A Brief Overview. *Energies* **2022**, *15*, 1563.

(18) Fu, Z.; Zhu, J.; Barghi, Sh.; Zhao, Y.; Luo, Z.; Duan, Ch. On the two-phase theory of fluidization for Geldart B and D particles. *Powder Technol.* **2019**, *354*, 64–70.

(19) Chiba, T.; Kobayashi, H. Gas exchange between the bubble and emulsion phases in gas-solid fluidized beds. *Chem. Eng. Sci.* **1970**, *25* (9), 1375–1385.

(20) Nemati, N.; Rydén, M. Chemical-looping combustion in packed-fluidized beds: Experiments with random packings in bubbling bed. *Fuel Process. Technol.* **2021**, *222*, 106978.

(21) Aronsson, J.; Pallarès, D.; Lyngfelt, A. Modeling and scale analysis of gaseous fuel reactors in chemical looping combustion systems. *Particuology* **2017**, *35*, 31–41.

(22) Aronsson, J.; Krymarys, E.; Stenberg, V.; Mattisson, T.; Lyngfelt, A.; Rydén, M. Improved Gas–Solids Mass Transfer in Fluidized Beds: Confined Fluidization in Chemical-Looping Combustion. *Energy Fuels* **2019**, *33* (5), 4442–4453.

(23) Song, X.; Wang, Z.; Jin, Y.; Tanaka, Z. Gas-solids circulating fluidization in a packed bed. *Powder Technol.* **1995**, *83* (2), 127–131.

https://doi.org/10.1021/acs.energyfuels.2c00527
Energy Fuels XXXX, XXX, XXX–XXX

(24) Sutherland, J. P.; Vassilatos, G.; Kubota, H.; Osberg, G. L. The effect of packing on a fluidized bed. *AIChE J.* **1963**, *9*, 437−441.
(25) Aronsson, J.; Pallarès, D.; Rydén, M.; Lyngfelt, A. Increasing Gas−Solids Mass Transfer in Fluidized Beds by Application of Confined Fluidization—A Feasibility Study. *Appl. Sci.* **2019**, *9*, 634.
(26) Gabor, J. D.; Mecham, W. J. *Engineering Development of Fluid-Bed Fluoride Volatility Processes, Part 4. Fluidized-Packed Beds: Studies of Heat Transfer, Solid Gas Mixing, and Elutriation*; Argonne National Laboratory: Lemont, IL, 1965; AEC Research and Development Report ANL-6859, pp 1−127, DOI: 10.2172/4588288.
(27) Verver, A. B.; van Swaaij, W. P. M. The heat-transfer performance of gas—solid trickle flow over a regularly stacked packing. *Powder Technol.* **1986**, *45* (2), 133−144.
(28) Nemati, N.; Andersson, P.; Stenberg, V.; Rydén, M. Experimental Investigation of the Effect of Random Packings on Heat Transfer and Particle Segregation in Packed-Fluidized Bed. *Ind. Eng. Chem. Res.* **2021**, *60* (28), 10365−10375.
(29) Mandal, D.; Sathiyamoorthy, D.; Vinjamur, M. Heat Transfer Characteristics of Lithium Titanate Particles in Gas-Solid Packed Fluidized Beds. *Fusion Sci. Technol.* **2012**, *62* (1), 150−156.
(30) Roes, A. W. M.; Van Swaaij, W. P. M. Axial dispersion of gas and solid phases in a gas—solid packed column at trickle flow. *Chem. Eng. J.* **1979**, *18* (1), 13−28.
(31) Donsì, G.; Ferrari, G.; Formisani, B. Expansion behaviour of confined fluidized beds of fine particles. *Can. J. Chem. Eng.* **1989**, *67*, 185−190.
(32) Girimonte, R.; Vivacqua, V. The expansion process of particle beds fluidized in the voids of a packing of coarse spheres. *Powder Technol.* **2011**, *213* (1), 63−69.
(33) Roes, A. W. M.; Van Swaaij, W. P. M. Hydrodynamic behaviour of a gas—solid counter-current packed column at trickle flow. *Chem. Eng. J.* **1979**, *17* (2), 81−89.
(34) Claus, G.; Vergnes, F.; Goff, P. L. Hydrodynamic study of gas and solid flow through a screen-packing. *Can. J. Chem. Eng.* **1976**, *54*, 143−147.
(35) Berguerand, N.; Lyngfelt, A.; Mattisson, T.; Markström, P. Chemical Looping Combustion of Solid Fuels in a 10 kW_{th} Unit. *Oil Gas Sci. Technol.* **2011**, *66* (2), 181−191.
(36) Kunii, D.; Levenspiel, O. *Fluidization Engineering*, 2nd ed.; Butterworth-Heinemann, Oxford, U.K., 1991; pp 1−210, DOI: 10.1016/C2009-0-24190-0.
(37) Engineering ToolBox. *Air—Diffusion Coefficients of Gases in Excess of Air*; Engineering ToolBox, 2018 (accessed Sept 7, 2021).
(38) Nemati, N.; Zarghami, R.; Mostoufi, N. Investigation of Hydrodynamics of High-Temperature Fluidized Beds by Pressure Fluctuations. *Chem. Eng. Technol.* **2016**, *39* (8), 1527−1536.
(39) Andersson, P. Experimental Determination of Heat Transfer Coefficient to Horizontal Tube Submerged in Packed-Fluidized Bed. M.Sc. Thesis, Department of Space, Earth and Environment, Chalmers University of Technology, Göteborg, Sweden, 2020.

https://doi.org/10.1021/acs.energyfuels.2c00527
Energy Fuels XXXX, XXX, XXX−XXX